Title

Toroidal rotation profile structure in KSTAR L-mode plasmas with mixed heating by NBI and ECH

Journal

Nuclear Fusion, 56(1)

ISSN

0029-5515

Authors

Shi, YJ
Ko, SH
Kwon, JM
et al.

Publication Date

2016

DOI

10.1088/0029-5515/56/1/016014

Toroidal rotation profile structure in KSTAR L-mode plasmas with mixed heating of NBI and ECH

[a,b,c]Y.J. Shi, [a]S.H.Ko, [a]J.M. Kwon, [a]W.H. Ko, [d]P.H. Diamond, [a]S. Yi, [e]K. Ida, [a]K.D. Lee, [a]J.H. Jeong, [a]S.H.Seo, [a]S.H.Hahn, [a]S.W. Yoon, [a]Y.S. Bae, [a]L.Terzolo, [f]G.S.Yun, [g]M. Bitter, [g]K. Hill

[a] National Fusion Research Institute, Daejeon, Korea
[b] Seoul National University, Seoul, Korea
[c] University of Science and Technology of China, Hefei, China
[d] CMTFO and CASS, University of California, San Diego, USA
[e] National Institute for Fusion Science, ,Japan
[f] Pohang University of Science and Technology, Pohang, Korea
[g] Princeton Plasma Physics Laboratory, Princeton, USA

Email: yjshi@ipp.ac.cn

Abstractor: The toroidal rotation profile structure with mixed heating of NBI and ECH has been investigated in KSTAR L-mode plasmas. ECH with varying resonance conditions were used for the heating mix and turbulence population control. The experimental results show that ECH causes a counter-current rotation increment both in off-axis and on-axis ECH heating. Off-axis ECH can produce larger counter-current rotation than the on-axis ECH for L-mode plasmas. One possible mechanism of the counter-current intrinsic torque with ECH is due to a transition from a state of ITG turbulence to CTEM turbulence, and thus a change in the sign of the turbulence driven residual stress. The linear gyrokinetic analyses show the ITG→TEM transition occurs in some region during ECH injection. Coordinated 1D transport analysis for ion heat and momentum of ECH L-mode plasmas shows the electron temperature gradient is the main driving force for the degradation of ion confinement and non-diffusion momentum flux.

1. Introduction

Toroidal plasma rotation is important for the control of stability and transport in tokamaks. Neutral beam injection (NBI), which is used widely to control plasma rotation in today's

tokamaks, is not a feasible approach for ITER and future reactor. It is necessary to explore alternative or complementary methods for driving plasma rotation. Significant intrinsic rotation (without external momentum input) has been observed on many tokamaks [1], which suggest that it may be possible to reap the benefits of such self-generated flows in ITER and reactors. Since the discovery of intrinsic rotation in the 1990s [2, 3], plasma rotation without external torque has been a hot topic. While significant progress has been made, the driving mechanisms are not fully understood. Theoretical models have been proposed to explain intrinsic rotation as due to a turbulence driven intrinsic torque [4-7]. Intrinsic torque is dynamic and variable – due to evolving turbulent Reynolds stresses. Momentum transport bifurcations and reversals have been observed in several experiments [8, 9].

The effects on toroidal rotation of ECH have being observed previously in many machines [10-18]. The counter-current rotation increment or flattening of co-current rotation profile was confirmed in these ECH experiments. The proposed explanations vary considerably.

The tendency of confined tokamak plasmas to self-accelerate to a state of intrinsic rotation has been identified and related to the conditions of plasma confinement. Intrinsic rotation is self-generated by ambient turbulence via the non-diffusive residual stress [4]. This, then, motivates the question of how macroscopic rotation profiles will evolve in response to changes in the ambient micro-turbulence. One ‘control knob’ for the micro-turbulence population is the heating mix of NBI (heats ion, and so drives ITG) and ECH (heats electrons, and so can drive CTEM).

The KSTAR results in this paper, though partly similar to some previous experiments, will be combined with gyrokinetic stability analyses and experimental results to elucidate possible physics mechanisms for ECH rotation experiments. In this work, we report the results of L-mode toroidal rotation experiments in 2013 KSTAR campaign. ECH with varying resonance conditions were used for the heating mix and turbulence population control. The experimental

data show that off-axis ECH can produce larger counter-current rotation than the on-axis ECH for L-mode plasma. From the detailed measurement of toroidal rotation and gyrokinetic micro-stability analysis, it was found that there is a strong correlation between the counter-direction torque by ECH and ITG→TEM turbulence population change.

This paper is organized as follows: The main experiment results about rotation structures are described in section 2. 1D transport analyses for heat and momentum are shown in section 3. Discussion about possibilities to explain the rotation behavior is presented in section 4. Gyro-kinetic analysis of stability is given in section 5. Conculusion and future plan are summarized in section 6.

2. Experimental results about rotation profiles

All the results presented in this paper were obtained in the KSTAR superconducting tokamak [19]. The charge exchange recombination spectroscopy (CES) [20] in KSTAR is the one of main diagnostics for the measurement of ion temperature (Ti) and toroidal rotation velocity (Vϕ), which had 32 toroidal lines of sights and can provided the whole plasma profiles from the plasma edge to the magnetic axis. X-ray imaging crystal spectrometer (XICS) [21] in KSTAR also can measure Ti and Vϕ. Unfortunately, XICS in KSTAR can only provide one channel data for core plasma in last two years. The profile data of Ti and Vϕ in this paper is only from CES. Electron temperature was measured with electron cyclotron emission radiometer (ECE) [22].The line averaged density measurements are based on the micro-wave interferometer and thus give indications of only the line averaged values. The micro-wave reflectometry [23] provided the density profiles for some shots in this paper.

NBI is the main heating power in KSTAR. On-axis 1.4 MW NBI (90~95keV) [24] were always injected in co-current direction during flap-top in the discharges presented here. There are two ECH heating system in KSTAR [25]. One is 110GHz (source power 0.5MW) and the other is

170GHz (source power 1MW). The experimental data in this paper is obtained with 170 GHz ECH heating. The ECH system was configured for X-mode second harmonic and deposition location was set using steerable mirrors in real time mode.

It is well known that ECH has very good localized electron heating effect. So ECH can be applied as the 'control knob' for the micro-turbulence population in dedicated resonance plasma region for the mixed heating scenario with NBI. In order to clarify the ECH effects on rotation profile structure, several identical discharges with same plasma parameters were selected for analysis. The main plasma parameters for these discharges are I_p = 0.6MA, B_T= 3T. The line-averaged density is about $1.5\times10^{19}m^{-3}$. Discharges were operated in double or quasi-double null configuration. Plasma elongation factor is about 1.8. The edge safety factor (q_{95}) is about 9 during flat-top phase. Only ECH working mode is different in these discharges. In our experiment, there are two working mode of ECH. The first one is ECH power modulation with fixed resonance layer in one shot (here, we call it modulated ECH plasma). The second mode is resonance layer scan with fixed power in one shot (here, we call it static ECH plasma).

Fig.1 shows the waveforms of two modulated ECH shots. The 5Hz modulated ECH pulses with 50% duty cycle are injected at the flop-top of NBI heating plasma. All the static plasma parameters and heating power in the two modulated ECH plasma are identical except the ECH resonance layer. The resonance layer of ECH is set as ρ=0.15 for on-axis heating and ρ=0.55 for off-axis heating. The modulated ECH power kept about 700kW in whole phase. The short beam-off blip of NBI is just used for the subtraction of background signal of CES. The beam-off time is only several milliseconds, which has a neglected effects for the experiment presented here. It is clear shown that increment of core electron temperature of on-axis ECH is much higher than that of off-axis ECH. Although the main effect of ECH is heating electron, it can be seen in fig.1 that the density, ion temperature and rotation velocity are also modulated with ECH. The line averaged density always increase slightly both for on-axis and off-axis ECH.

On the other hand, both Ti and Vϕ decrease during ECH injection. Especially, both CES data and XICS data show that the decreased amplitude of Vϕ of off-axis ECH is bigger than that of on-axis ECH.

The ECH resonance layer effect on rotation was also investigated in static ECH plasma. All the parameters of static plasma are same with the modulated ECH plasma. In static ECH plasma, the ECH resonance layer is start from ρ=0.15 and scan from ρ=0.15 to ρ=0.55 in 2s during the flattop of one discharge. Fig.2 shows the rotation profiles of static ECH plasma. It can be seen in fig.2 that the off-axis ECH make larger rotation reduction than the on-axis ECH, which is consist with the modulated ECH plasma. The line averaged density increase induced by ECH is also observed in static ECH plasma. The density profiles of static ECH plasma measured with micro-wave reflectometry are shown in fig.3. Although, the density in ECH phase is higher than that in NBI phase, the shape or the gradient of density profile is not change. At the same time, the density profile of on-axis ECH is almost same as that of off-axis ECH. So density effect on rotation for the experiment in this paper can be removed.

The modulated amplitudes and phase delay of temperature and toroidal rotation velocity with FFT analysis for modulated ECH plasma presented in fig.1 are shown in fig.4. The modulated amplitudes of Te in fig.5c clear indicated the localized heating effect of ECH. Although the location of maximum value of δTe both for on-axis and off-axis case is a little more inside than the pre-setted ECH resonance position, the on-axis heating effect and off-axis heating effect are quite clear and achieved.

On the other hand, both the amplitude of δTi and phase delay of Ti (ϕ_{Ti}) for on-axis ECH case is very close to those for off-axis ECH case. The small hump of δTi in off-axis ECH in fig.5b is also coincident with the positon of maximum δTe. On the other hand, the relation between δVϕ and ECH layer is in contrast to the relation between δTi and ECH layer. Fig.5a clear shows that δVϕ in off-axis ECH is much higher than that in on-axis ECH, which is agree with the

static ECH results in fig.2. It can be also observed that phase delay of Vϕ ($\phi_{V\phi}$) are larger than ϕ_{Te} and smaller than ϕ_{Ti} in the whole region, which means the change of Vϕ is behind the change of Te and faster than the change of Ti. On the other hand, ϕ_{Ti} gradually increases with minor radius, while $\phi_{V\phi}$ is quite flat in ρ<0.8 region. For the ρ>0.8 region, the error-bars of $\phi_{V\phi}$ and ϕ_{Ti} are too larger to investigate the evolution of δV and δTi.

3. 1D transport analyses for heat and momentum for modulated ECH plasma

In this part, we'd like to present more detailed transport analyses for modulated ECH L-mode experiment to identify the mechanisms of the momentum and heat transport changes. One novel target in our 1D transport is the calculation of non-diffusion momentum terms. Both intrinsic torque (such as residual stress) or damping and pinch can contribute to the non-diffusion momentum flux. Firstly, the ion heat balance equations are written as

$$\boldsymbol{n_i \frac{\partial T_i}{\partial t} = -\nabla \cdot \vec{q} + Q} \qquad \textbf{(1)}$$

$$\boldsymbol{\vec{q} = -n_i \chi_i \frac{\partial T_i}{\partial r}} \qquad \textbf{(2)}$$

where n_i, χ_i , $\vec{q}$ and Q are the ion density, the ion heat conductivity, the ion heat flux and NBI heating source, respectively. Secondly, the toroidal momentum balance equations can be written as

$$m_i \frac{\partial n_i V_\phi}{\partial t} = -\nabla \cdot \Pi + F \quad (3)$$

$$\boldsymbol{\Pi} = -m_i \chi_\phi \frac{\partial n_i V_\phi}{\partial r} + \Pi_{non-diff} \quad (4)$$

where m_i, χ_ϕ , F, Π and $\Pi_{non\text{-}diff}$ are the ion mass, the momentum diffusion coefficient, the external NBI torque, the total momentum flux and non-diffusion momentum flux, respectively. NBI heat source and torque are calculated with NUBEAM code [26]. The measured values of the density, temperature and rotation velocity are applied for this transport analysis. In the first step, χ_i can be obtained from the heat balance equation. In the next step, χ_ϕ is determined with some assumption. For the L-mode plasma, one general assumption [27] is $\chi_\phi = \chi_i$, i.e. Prandtl number $P_r = \chi_\phi/\chi_i = 1$. Then, the non-diffusion momentum item $\Pi_{non\text{-}diff}$ can be obtained from th

e momentum balance equation. On the other hand, there also some observations or theory to s upport Prandtl number varying in certain range [13, 28-29]. Here, the transport analysis results for P_r = 0.75 and P_r =1.25 are also presented.

Both χ_i and $\Pi_{non\text{-}diff}$ are calculated at two radial positions. Figure 5 show the results of ion heat transport analysis. The notable character of χ_i is that it increase with injection of ECH, which means the degradation of ion heat confinement by ECH. On the other hand, χ_i shows very dif ferent response to the ion and electron temperature gradient (∇Ti and ∇Te) changes. As the ∇ Te increases with ECH, χ_i increase in these radial locations. Moreover, clear hysteresis loop b etween χ_i and ∇Te is shown in Figure 5, which is mainly due to the time lag between the two quantities (∇Te change first, then χ_i change). These evidences clear indicate that the electron temperature gradient is the main driving source of ion heat transport. On the other hand, the co rrelation between χ_i and ∇Ti shows different behavior (χ_i decreases with ∇Ti). This opposite t rend can be understood as a response of plasma to dispose a fixed NBI heating power with var ying ion heat conductivities. (i.e. recall that in steady state $-\frac{\partial T_i}{\partial t} = -\chi_i \frac{\partial T_i}{\partial r} + P_{NBI} = 0$ ➔ $\chi_i \propto P_{NBI} \left(\frac{\partial T_i}{\partial r}\right)^{-1}$).

The analysis results of $\Pi_{non\text{-}diff}$ are shown in figure 6. The relation of $\Pi_{non\text{-}diff}$ with ∇Ti and ∇Te is similar as the relation of χ_i with ∇Ti and ∇Te. Three cases for P_r=0.75,1.0 and 1.25 are presented in fig.6. The evolution trends of $\Pi_{non\text{-}diff}$ are same for the three Prandtl numbers except the absolute value of $\Pi_{non\text{-}diff}$. $\Pi_{non\text{-}diff}$ increase with ∇Te and decrease with ∇Ti, which implies that the electron temperature gradient is the main driving force of this non-diffusive momentum. At the same time, the stronger hysteresis between $\Pi_{non\text{-}diff}$ and ∇Te also implies a time lag between them. ECH induces the rapid steepening of electron temperature profile first and the changes of non-diffusive momentum flux follow the change of ∇Te. On the other hand,

the ion temperature gradient shows relatively weak and less clear hysteresis trends with $\Pi_{non-diff}$.

The correlation between the non-diffusive momentum flux and the toroidal rotation itself has a lso investigated (as shown in figure 7). Unlike the clearly proportionality between the moment um flux and electron temperature gradient, these figures show no such clear proportionality. A s mentioned in form text, both intrinsic torque or damping and pinch may contribute to the no n-diffusion momentum flux. The momentum flux from the pinch contribution should be propo rtional to the toroidal rotation velocity. This observation suggests that momentum pinch canno t explain this non-diffusive momentum flux alone.

4. Discussion about damping and torque in ECH plasma

There two possible explanation for the ECH induced counter-current increment of toroidal rotation. One explanation is that some damping effects induced by ECH reduce the rotation velocity. The other is that some counter-current torque produced by ECH contribute to the counter-current increase of $V\phi$. One damping mechanism the neoclassical toroidal viscosity (NTV) damping effect [30, 31]. However, any violent MHD (such as sawtooth, kink mode, and NTM, etc…) activity cannot be observed during ECH injection in the experiment presented here. High safety factor ($q_{95} \sim 9$) discharge was designed to avoid intense MHD behavior in this paper. So NTV damping effect can be neglected in our experiment. The other damping force for the rotation is the degeneration of ion confinement. But the change amplitude of Ti is almost same for on-axis and off-axis ECH. So the evolution of $V\phi$ should also be similar for on-axis and off-axis ECH if the worse ion confinement during ECH is the main force, which is not consist with the experimental result. So, counter-current torque induced by ECH is very high possibility to support the experiment results in this paper. Actually, it has been already observed that the central rotation changes its sign from co- to counter-current direction during high power ECH injection for the NBI+ECH plasma in LHD [32], which is the powerful evidence that the

effect of ECH is not damping the rotation but driving force in counter-direction. At present, the ECH power in KSTAR is still too low. Rotation reversal by ECH in KSTAR is expected if the ECH power is high enough in future experiment.

The turbulence mode transition from TEM to ITG, and thus a change in sign of the residual str ess, is one of the strong candidate mechanisms for the counter-current torque by ECH [4-6]. T he detail analysis of turbulence status for the NBI+ECH plasma in KSTAR is presented in nex t section.

5. Gyro-kinetic linear stability analysis

Since residual stress is affected by characteristics of ambient residual micro-instabilities such as mode propagation direction and strength of excitation, we carry out linear micro-instability analysis using GYRO. GYRO is popularly used for linear and nonlinear micro-instability simulations [33, 34]. From 1-D transport analysis, we find that the change of T_e according to ECH injection is a "control knob" of ion heat and toroidal momentum transport, and this implies that a ρ_i-scale micro-instability, which is excited by electron temperature gradient, could have a role in the transport and one candidate of micro-instabilities is trapped electron mode (TEM).

For linear GYRO analysis, we use density, ion and electron temperature and toroidal rotation profiles at the same times when profiles in Fig. 2 was measured. In addition to free energies of radial profiles, trapped electron fraction is important for excitation of TEM and it depends on magnetic geometry i.e. shape of magnetic flux surface. Collision also affects TEM by hindering path of trapped electron. All these effects are considered simultaneously in the analysis, and we focus on electro-static micro-instabilities. Fig. 2 shows that toroidal rotation during ECH injection changes mainly around core region ($\rho \leq 0.8$) of plasmas. We also calculate micro-instabilities on this region.

Fig. 8 shows results of linear GYRO analysis for three different cases, NBI heated L-mode plasma, NBI + on-axis ECH heated L-mode plasma, and NBI + off-axis ECH heated L-mode plasma. For NBI heated L-mode plasma, ion temperature gradient mode (ITG), which propagates along ion diamagnetic direction, is dominantly excited in almost whole core region. For NBI + on-axis ECH heated L-mode plasma, dominant micro-instability changes from ITG to TEM. By heating additionally on electron, trapped electron mode is excited in whole core region of plasma. It could support that residual stress change comes from population change of dominant micro-instability i.e. from ITG to TEM. For NBI + off-axis ECH heating L-mode plasma, TEM is excited on only limited region of plasma from ρ=0.5 to ρ=0.8. TEM is more strongly excited than TEM of NBI + on-axis ECH heating, because trapped electron fraction increases as r increases. It may explain that even though off-axis ECH is less efficient to heat electron than on-axis ECH, off-axis ECH is more effective to exert counter torque and slow-down toroidal rotation.

In this study, we glance through tendency of linear micro-instabilities that profiles of three different heating cases have, but in real situation, ambient residual micro-instabilities should be determined as nonlinear processes. We would remain nonlinear study of micro-instabilities as future works.

6. **Summary and future plans**

ECH always induce counter-current rotation change both in on-axis and off-axis ECH plasma in KSTAR**.** For L-mode plasmas, off-axis ECH induces stronger counter-current increment than on-axis ECH. The experimental results highly support that the effect of ECH is not damping the rotation but torque in counter-direction. The change of the turbulence mode (ITG-TEM) is

the strong candidate mechanisms for the counter-current torque, which is also indicated as the main mechanism in ECH effects on rotation for the H-mode plasmas in AUG [13-14] and KSTAR [15]. Linear gyro-kinetic analyses indicate that off-axis ECH causes stronger excitation of TEM at outer region, while on-axis ECH mainly excite TEM at inner region, which is consistent with macro-trend of $\Delta V\phi$. 1D transport analysis shows the clear correlation that both χi and $\Pi_{non\text{-}diff}$ incease with ∇Te, which indict electron temperature gradient is main driver for the heat and momentum transport.

In the future KSTAR experiments, more higher ECH power and power ratio of P_{ECH}/P_{NBI} will be applied to achieve zero or negative core toroidal rotation. Density profile evolution is clearly critical to this study, and a satisfactory explanation of the peaking phenomenon is as yet elusive. Momentum and particle transport are coupled and must be studied together. Some core fluctuation diagnostics, such as BES and ECEI in KSTAR, will be used widely for the directly experimental turbulence mode investigation coordinated with macroscopic analysis. It is very critical need to develop the nonlinear gyrofluid simulations of dynamically interacting domains and competing flux driven ITG and TEM turbulence.

6. Acknowledgments

The authors thank the participants in the 4th APTWG workshop, 25th IAEA FEC and 13th Transport and Confinement Topic Group Meeting of ITPA for helpful discussions and encouragement. This work was partly supported by the World Class Institute (WCI) Program of the National Research Foundation of Korea (NRF) funded by the Ministry of Education, Science and Technology of Korea (MEST) (NRF Grant No. WCI 2009-001) and Brain Korea 21 Program for Leading Universities & Students (BK21 PLUS).

References

[1] Rice J. E. *et al* 2007 *Nucl. Fusio*n **47** 1618
[2] Ida K. *et al* 1991 *Nucl. Fusion* **31** 943
[3] Rice J. E. *et al* 1998 *Nucl. Fusion* **38** 75

[4] Diamond P. H. *et al* 2008 *Phys. Plasmas* **15** 012303
[5] Gurcan O. D. *et al* 2007 *Phys. Plasmas* **14** 042306
[6] Kwon J. M. *et al* 2012 *Nucl. Fusion* **52** 013004
[7] Camenen Y. *et al* 2011 *Nucl. Fusion* **51** 073039
[8] Bortolon A. *et al* 2006 *Phy. Rev. Lett* **97** 235003
[9] Rice J. E. *et al* 2011 *Phy. Rev. Lett* **107** 265001
[10] Ida K. *et al* 2001 *Phy. Rev. Lett* **86** 3040
[11] deGrassie J S *et al* 2004 *Phys. Plasmas* **11** 4323
[12] Yoshida M. et al 2009 *Phy. Rev. Lett* **103** 065003
[13] McDermott R. M. *et al* 2011 *Plasma Phys. Control. Fusion* **53** 035007
[14] Angioni C. *et al* 2011 *Phy. Rev. Lett* **107** 215003
[15] Shi Y.J. *et al* 2013 *Nucl. Fusion* **53** 113031
[16] Sakamoto Y., *et al* 2006 *Plasma Phys. Control. Fusion* **48** A63
[17] deGrassie J S *et al* 2007 *Phys. Plasmas* **14** 056115
[18] Porte L. *et al* 2007 *Nucl. Fusion* **47** 952
[19] Lee G. S. *et al* 2000 *Nucl. Fusion* **40** 575
[20] Ko W. H. *et al* 2010 *Rev.Sci.Instrum.* **81** 10D740
[21] Lee S.G. *et al* 2010 *Rev. Sci. Instrum.* **81** 10E506
[22] Jeong S. H. *et al* 2010 *Rev.Sci.Instrum.* **81** 10D922
[23] Seo S.H. *et al* 2012 *Rev.Sci.Instrum.* **83** 10E342
[24] Bae Y. S. *et al* 2012 *Fusion Engineering and Design* **87** 1597
[25] Bae Y. S. *et al* 2014 *Fusion Science and Technology* **65** 88
[26] Pankin A. *et al* 2004 *Computer Physics Communications* **159** 157
[27] Diamond P. H. *et al* 2013 *Nucl. Fusion* **53** 104019
[28] Casson F. J. *et al* 2009 *Phys. Plasmas* **16** 092303
[29] Peeters A. G. *et al* 2011 *Nucl. Fusion* **51** 094027
[30] Shaing K.C. 2003 *Phys. Plasmas* **10** 1443
[31] Seol J.S. *et al* 2012 *Phy. Rev. Lett* **109** 195003
[32] Ida K. *et al* 2015 *Nucl. Fusion* **55** 017001
[33] Candy J and Waltz R E 2003 *J. Comput. Phys.* **186** 545
[34] Candy J and Waltz R E 2003 *Phys. Rev. Lett.* **91** 045001

Figure Captions

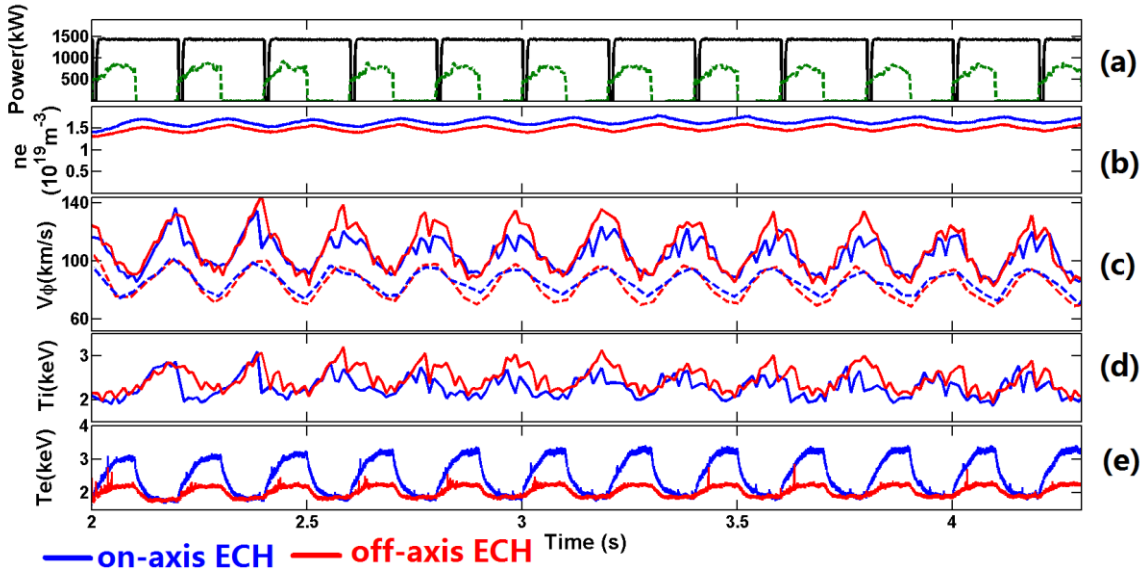

Figure.1 waveforms of modulated ECH L-mode discharge. From top to bottom are: (a) Heating power, (b) line-averaged density, (c) core toroidal rotation velocity measured by CES (solid line) and XICS (dashed line) (d) core ion temperature, (e) core electron temperature.

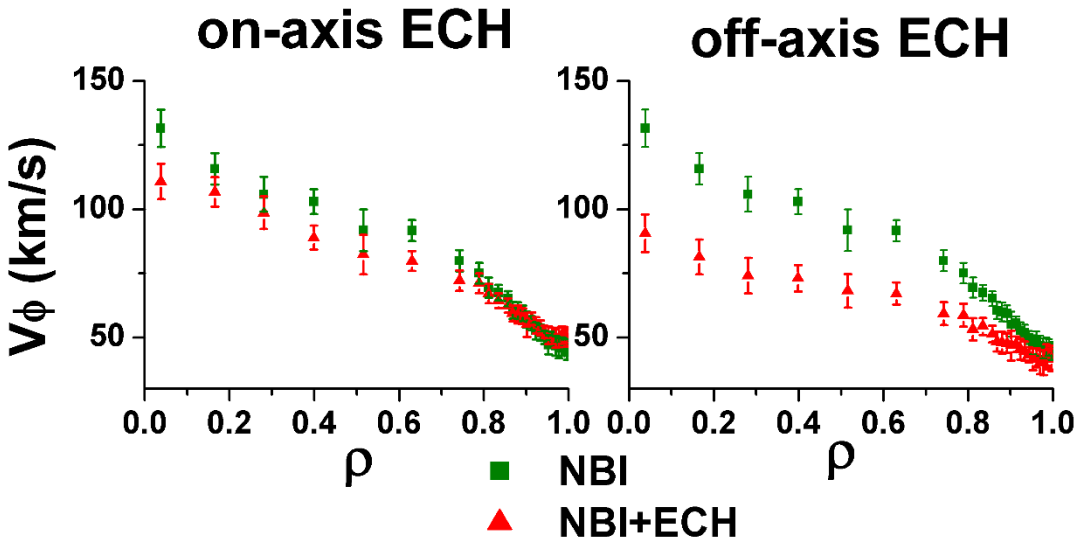

Figure.2 Profiles of rotation velocity in static ECH+NBI L-mode plasma

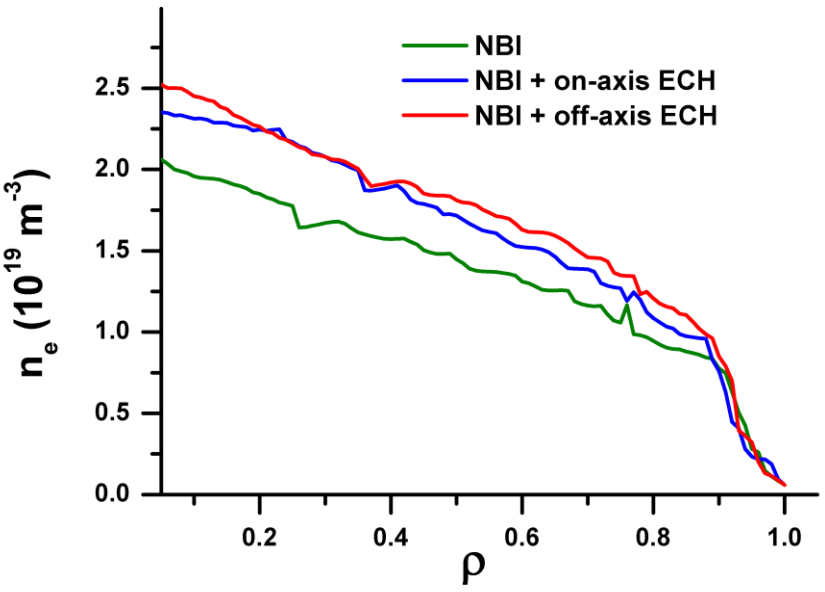

Figure.3 The density profiles for static ECH+NB L-mode plasma

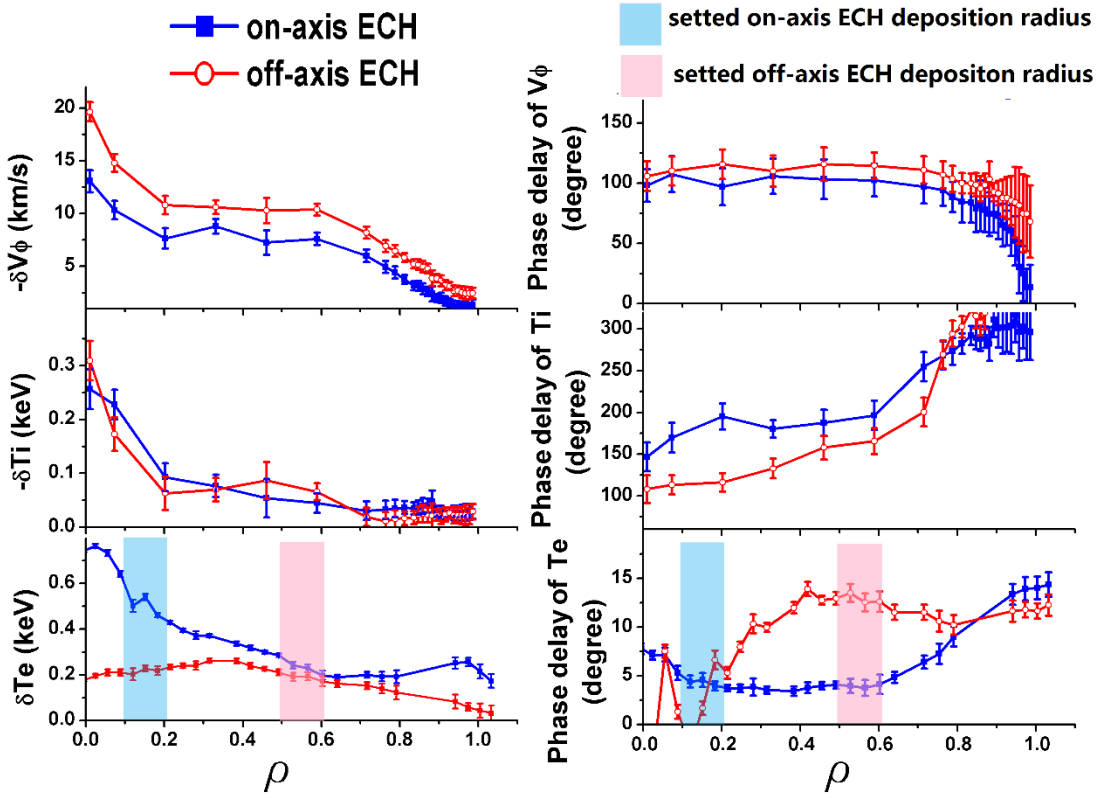

Figure.4 Profiles of modulated amplitudes and phase delay of Vϕ (up), Ti(middle) and Te(bottom) in the discharges in figure.2

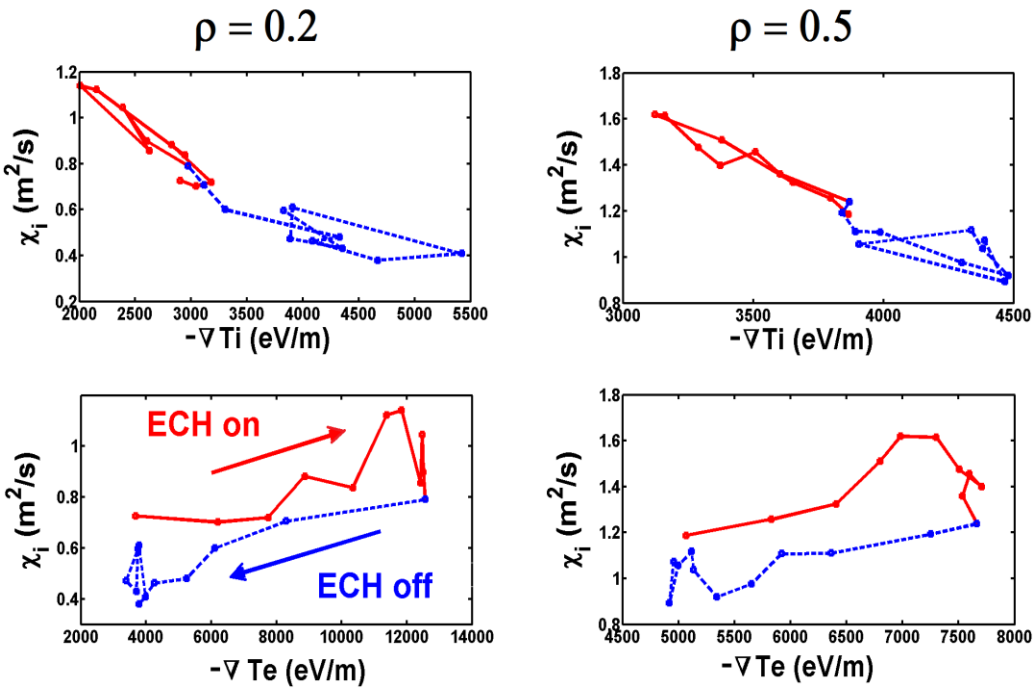

Figure.5 The relation between ion heat conductivity and temperature gradient at two radial positon..Up pannel: χ_I v.s ∇Ti. Down pannel: χ_I v.s ∇Te. From fig.6 to fig.8, the individual points are corresponding with the time points in one ECH modulation cycle. The time resolution of CES in KSTAR is 10ms. There are 20 time points in one ECH modulation cycle (200ms). Solid line represent ECH on phase, dashed line represent ECH off phase.

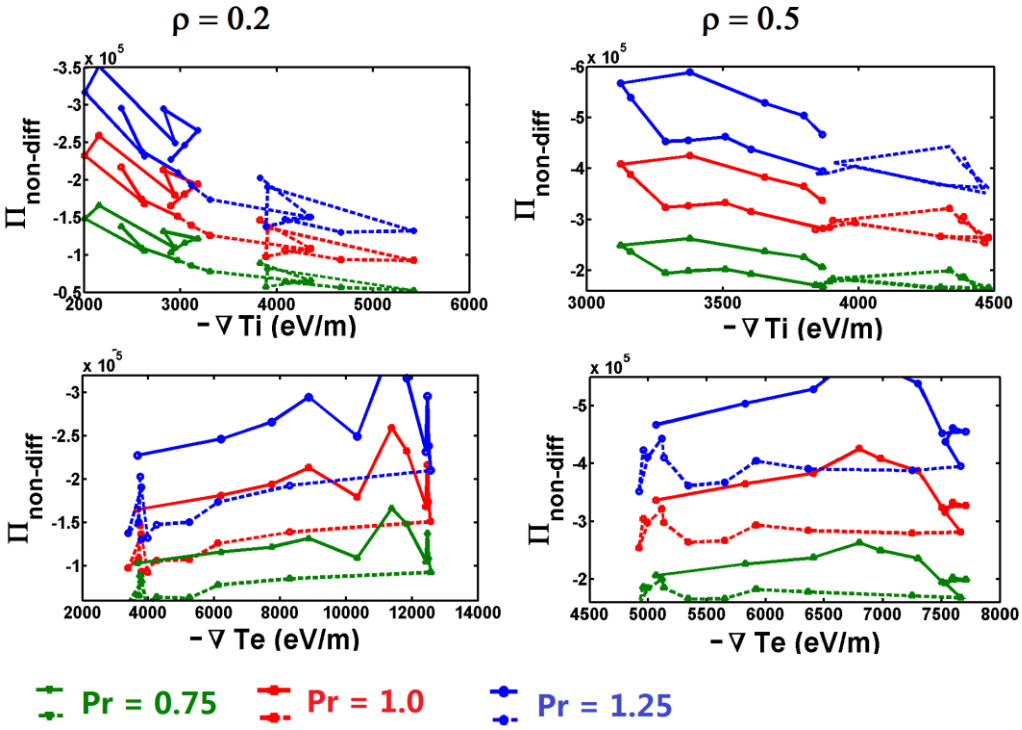

Figure.6 The relation between non-diffusive momentum flux and temperature gradient at two radial positon..Up pannel: $\Pi_{non\text{-}diff}$ v.s ∇Ti. Down pannel: $\Pi_{non\text{-}diff}$ v.s ∇Te. Solid line represent ECH on phase, dashed line represent ECH off phase.

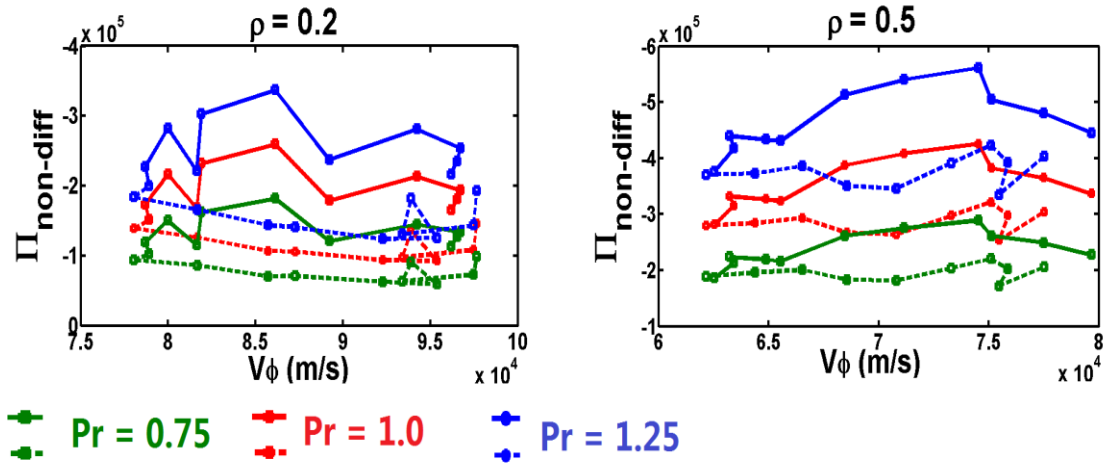

Figure.7 The relation between non-diffusive momentum flux and toroidal rotation velocity. Solid line represent ECH on phase, dashed line represent ECH off phase.

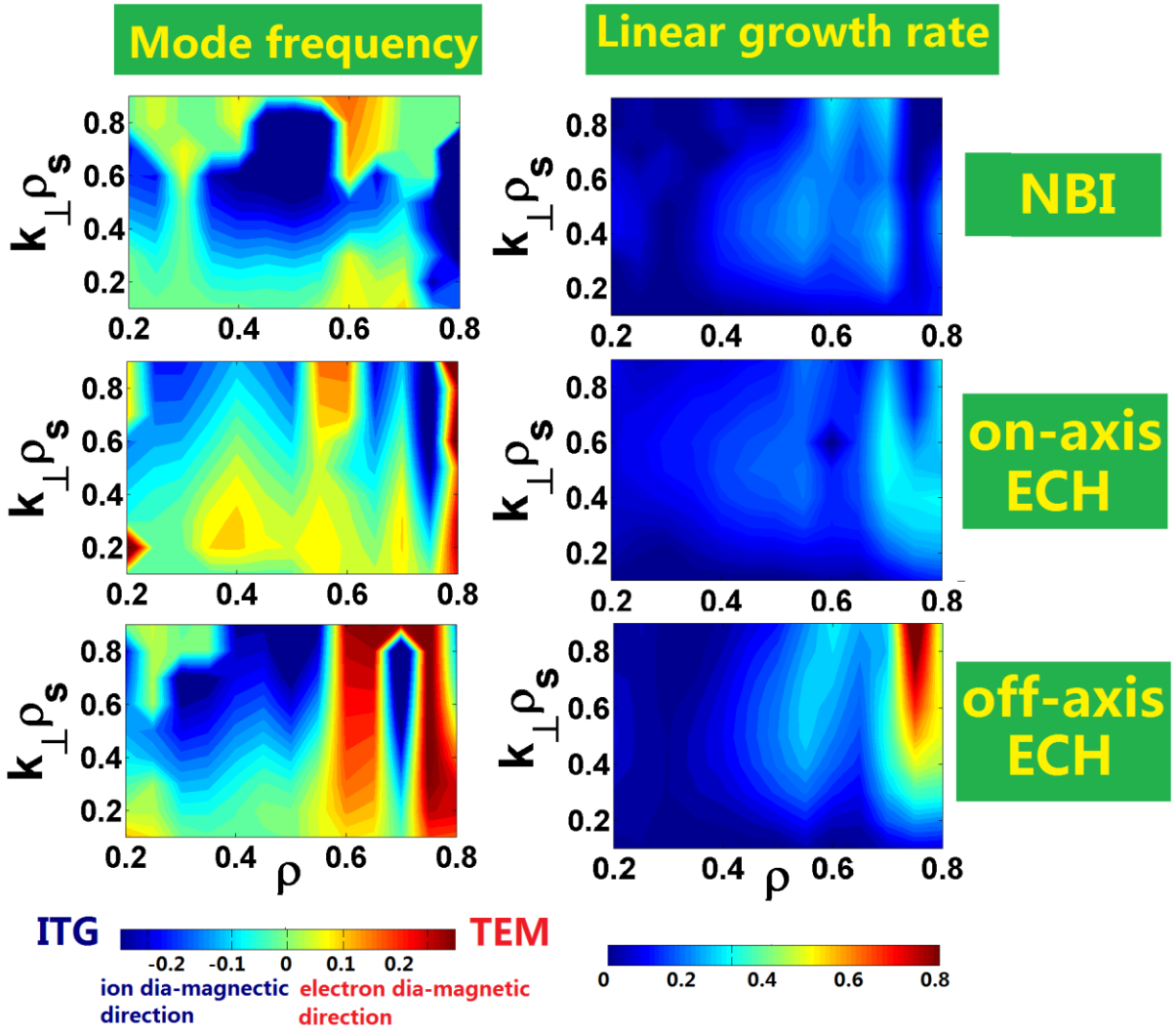

Figure.8 Profiles of mode frequency (left) and linear growth rate(right) simulated with GYRO. For the mode frequency, blue color represent ion diamagnetic direction, which means ITG turbulence mode, red color represent electron diamagnetic direction, which means TEM turbulence mode.